frontiers | Frontiers in Carbon

TYPE Original Research
PUBLISHED 05 February 2024
DOI 10.3389/frcrb.2024.1305183

OPEN ACCESS

EDITED BY
Duncan John Mowbray,
Yachay Tech University, Ecuador

REVIEWED BY
Sadegh Sadeghzadeh,
Iran University of Science and Technology, Iran
Pilgyu Kang,
George Mason University, United States

*CORRESPONDENCE
Solange B. Fagan,
solange.fagan@gmail.com

RECEIVED 30 September 2023
ACCEPTED 03 January 2024
PUBLISHED 05 February 2024

CITATION
de Matos CF, Leão MB, Vendrame LFO, Jauris IM, Zanella I and Fagan SB (2024), Unlocking the paracetamol adsorption mechanism in graphene tridimensional-based materials: an experimental-theoretical approach.
Front. Carbon 3:1305183.
doi: 10.3389/frcrb.2024.1305183

Unlocking the paracetamol adsorption mechanism in graphene tridimensional-based materials: an experimental-theoretical approach

Carolina F. de Matos[1,2], Mayara B. Leão[1], Laura F. O. Vendrame[3], Iuri M. Jauris[4], Ivana Zanella[3] and Solange B. Fagan[3]*

[1]Environmental Science and Technology Center, Campus Caçapava do Sul, Federal University of Pampa, Caçapava do Sul, Brazil, [2]Chemistry Department, Federal University of Santa Maria, Santa Maria, Brazil, [3]Physics Department, Franciscan University, Santa Maria, Brazil, [4]School of Sciences, Pontifical Catholic University of Rio Grande do Sul, Porto Alegre, Brazil

The omnipresence of emerging contaminants in the aquatic environment is indisputable. These contaminants include chemical substances not removed in traditional water and sewage treatment processes. To ensure the quality of water and healthy aquatic ecosystems, new treatment technologies and materials are essential to effectively control the presence of these contaminants in the aquatic environment. More than that, it is important to know how molecules interact with these new materials. A low-cost alternative currently available is adsorption. Despite this method being widely studied, describing the interaction mechanisms between the materials and the analytes is not usual, limiting the obtainment of more efficient materials. Thus, the objective of this work was to understand, in a theoretical-experimental way, the forms of interaction in the adsorption of the drug paracetamol, widely used worldwide, in materials based on graphene with different chemical and structural properties. For this, kinetic and isothermal experimental studies were carried out using four materials that contemplated different dimensions, pore sizes, and oxidation degrees. In theoretical studies, density functional theory (DFT) simulations were performed to cover quantum details, revealing how paracetamol interacts with different graphene structures. According to theoretical studies, binding energies, binding distances, and charge transfer between oxidized graphene and paracetamol drug are compatible with physical adsorption, strongly dependent on the type and number of functional groups on the graphene surface. These results agree with the experimental data where the highest adsorptions were observed precisely for materials containing a higher proportion of functional groups and where these groups are more available (more porous), with adsorptive capacities reaching 235.7 mg/g. Our findings

contribute to scientific knowledge about using graphene structures as an adsorbent material, providing a solid basis for future studies and developing more efficient and advanced water treatment technologies.

KEYWORDS

contaminants, density functional theory, functional groups, oxidized graphene, simulation

1 Introduction

Graphene, graphene oxide (GO), and reduced graphene oxide (2D-rGO) have been widely used as adsorbents to remove different classes of contaminants from water (Ersan et al., 2017; Bolisetty et al., 2019; Liu et al., 2019; Yousefi et al., 2019; Alves et al., 2021). This application is highlighted for this type of material due to its unique properties, such as high specific surface area and amphiphilic structure, in materials with polar groups (Alves et al., 2021; Huang et al., 2021). Pristine graphene, besides its limitations in obtaining (Wang et al., 2020), has limited applications due to its hydrophobicity and its unique π-π interactions. GO and rGO, on the other hand, improve the accessibility of contaminants in aqueous systems and extend material-analyte interactions through hydrogen bonding and electrostatic interactions (Deshwal et al., 2023; Fan et al., 2023). Despite the range of these materials in removing contaminants, their applications are limited by agglomeration or re-stacking of graphene sheets through strong π-π and van der Waals interactions between the sheets. This process results in a reduction in surface area, poor dispersion in aqueous media, and a consequent reduction in adsorption efficiency (Shan et al., 2017; Alves et al., 2021; Lin et al., 2021; Wong et al., 2022). In addition, due to their two-dimensional structure, these materials can be easily leached into water bodies, being affected by a difficult recovery process.

An alternative to solve these problems is using three-dimensional materials of reduced graphene oxide (3D-rGO). These materials have interconnected pores formed by the disorderly bonding of two-dimensional reduced graphene oxide sheets (Shan et al., 2017). These materials are a solution to the problems mentioned above and have excellent mechanical properties, specific surface areas, and high porosity (Torabi Fard et al., 2022). Based on their structures and properties, these materials have been applied in different contaminant removal methods, such as photocatalysis, advanced Fenton oxidation, capacitive deionization (Jung et al., 2018; Wang et al., 2019; Yang et al., 2020; Yu et al., 2022), and especially adsorption (Bruckmann et al., 2022; Leão et al., 2022; Leão et al., 2023). This water treatment method is widely used due to its simplicity and high efficiency (Hiew et al., 2019). In the case of three-dimensional graphene materials and their derivatives, relevant and desirable adsorptive capacities have been found for different contaminants (Torabi Fard et al., 2022), such as metals, dyes (Liu and Qiu, 2020; Lin et al., 2021; Sun et al., 2021), organic solvents, oils (Liu and Qiu, 2020; Wong et al., 2022), pesticides (Guo et al., 2021), and drugs. In the case of drugs, different classes have been removed through the adsorption process, using three-dimensional materials based on graphene, decorated or not. Recent studies show, for example, the use of three-dimensional reduced graphene oxide functionalized with caffeic acid in the removal of norfloxacin (220.99 mg g^{-1}) and ketoprofen (125.37 mg g^{-1}) (Lu et al., 2020); when functionalized with chitosan, a similar material was able to remove up to 14.4 mg g^{-1} of sulfamethazine (Hamed et al., 2022). The synergistic effects of 3D-rGO/MnO_2 were evaluated in removing and degrading tetracycline from water, which can remove up to 91% of this drug (Song et al., 2019). The 3D-rGO has also been applied to efficiently remove ibuprofen, diclofenac and naproxen with efficiencies of up to 526 mg g^{-1} (Umbreen et al., 2018).

Pharmaceutical products are not fully eliminated in conventional water and sewage treatments and are destined for water resources. There, they can impact the organisms that live in that ecosystem and humans (Villaescusa et al., 2011; Hamed et al., 2022). A drug that has attracted attention due to its characteristics is paracetamol (PCM), also known as acetaminophen, the most widely used analgesic worldwide (Villaescusa et al., 2011; van den Driesche et al., 2015; Hiew et al., 2022). When ingested, paracetamol cannot be completely metabolized, and approximately 20% of the drug is excreted into the environment as metabolites, ending up in water bodies and effluent treatment plants. During the disinfection process of water or effluents, paracetamol may be reactive with hypochlorite, generating significantly toxic compounds (Bedner and MacCrehan, 2006). In addition, several studies suggest that paracetamol may have endocrine-disrupting effects at all stages of human development, being able to act as an anti-androgenic substance and causing male reproductive disorders (van den Driesche et al., 2015; Albert et al., 2013; Kristensen et al., 2016; Kristensen et al., 2011; Kristensen et al., 2012). In addition to the wide use and risks attributed to this drug, there is also a low number of studies evaluating its removal using adsorption since conventional water treatment techniques (Villaescusa et al., 2011; Hamed et al., 2022). Paracetamol adsorption has been described on silica, alumina (Lorphensri et al., 2006), aquifer sand (Hamed et al., 2022), and carbon materials such as coconut activated carbon (Fernandez et al., 2015), rice husk (Paredes-Laverde et al., 2019), and tea leaves (Wong et al., 2018), grape stalk, yohimbe bark and cork bark (Villaescusa et al., 2011), multi-walled carbon nanotubes (Yanyan et al., 2018) and graphene oxide (Moussavi et al., 2016). At the same time, no studies report the use of graphene-based three-dimensional materials, which had their previously mentioned advantages.

Simultaneously, to find new materials capable of efficiently removing this drug, it is necessary to determine the interaction mechanisms between the material and the analyte. These determinations can be carried out using computer simulations, where one can simulate the interaction with materials that present different degrees of oxidation or pore sizes, for example,. In this sense, the objective of this work was to experimentally evaluate the efficiency of 3D-rGO materials with different degrees of oxidation of the structure and a two-dimensional graphene oxide material (2D-rGO) in the adsorption of the analgesic paracetamol.

Furthermore, the experimental results were compared with *ab initio* computer simulations to elucidate the mechanisms involved in the material-analyte interaction.

2 Experimental

2.1 Experimental setup and details

2.1.1 Obtaining 2D graphene-based material

Two-dimensional reduced graphene oxide was obtained from the chemical oxidation of graphite, followed by exfoliation to obtain graphene oxide. The reducing agent ascorbic acid was used at a concentration of 25 mmol L^{-1} 150 mL of GO dispersion (1 mg mL^{-1}) and the corresponding amount of reducing agent were added to a round bottom flask and kept at reflux for 3 h. At the end of the process, the material obtained was washed several times with distilled water.

2.1.2 Obtaining 3D graphene-based materials

The three-dimensional materials of reduced graphene oxide (3D-rGO) were obtained as described by Leão et al. (Leão et al., 2022), from the chemical oxidation of graphite followed by exfoliation in an ultrasound bath (SP Labor, model SP-UL, frequency 50 kHz) to obtain graphene oxide. A dispersion of this graphene oxide at a concentration of 1 mg mL^{-1} was used to obtain 3D-rGO. This was obtained from a thermochemical process using the ascorbic acid-reducing agent at different concentrations (0, 5, and 25 mmol L^{-1}). The corresponding amount of reducing agent and 50 mL of GO dispersion were added to 100 mL beakers, mixed, and taken to an autoclave (Stermax Digital Super Top, 21 L) at 120 C for 90 min. At the end of the process, the monoliths were removed and washed with distilled water, ready for use as a hydrogel. The entire synthesis process takes about 2 h.

The abbreviations for reference to the samples in this work are 3D-rGO for three-dimensional reduced graphene oxide. The second part of the acronym refers to different concentrations of reducing agent (0, 5 and 25 mmol L^{-1}); for example, 3D-rGO0 is used for 3D reduced material without ascorbic acid, and so on.

2.1.3 Materials characterization

The complete characterization of these materials is better described in our previous work (Leão et al., 2022). In this previously published work, the characterizations of X-ray Diffraction (XRD), Fourier Transform Infrared Spectroscopy (FTIR), Raman Spectroscopy, Thermogravimetry (TGA) and zero charge point pH (pH_{ZCP}) are presented. To avoid repetitions, in this work, the characterization of 3D-rGO0, 3D-rGO5, 3D-rGO25 and 2D-rGO was performed using Scanning Electron Microscopy (SEM), Brunauer–Emmett–Teller (BET) specific surface area values, and indirect potentiometric titration.

For Scanning Electron Microscopy, a MIRA 3 FEG-SEM microscope was used. The samples were placed on double-sided copper tapes previously glued on the sample holder. All samples were metalized with chromium; the source voltage was 15 kV. The BET method obtained the surface area using a Quantachrome Instrument, NOVA 4200e, United States. The indirect potentiometric titration was performed according to Hanelt et al. (2011) (Hanelt et al., 2011). The materials were kept in a NaOH 0.0025 mol L^{-1} solution, standardized with potassium biphthalate, for 24 h. At the end of this time, the solution was filtered and titrated with HCl 0.001 mol L^{-1}, using KCl 0.01 mol L^{-1} as a supporting electrolyte.

2.1.4 Adsorption experimental studies

The kinetic study used 8 mg of each material, left in contact with 5 mL of PCM 50 mg L^{-1}. At predetermined time intervals and until equilibrium, the concentration of PCM in the solution was determined. From the data obtained, the adsorptive capacity of the materials was calculated using Equation (1) (Thue et al., 2018), where Qe, is the adsorptive capacity in mg g^{-1}, Ce and Cf are the initial and final concentrations of the solution (mg L^{-1}), V is the volume of solution (L) and m is the mass of the adsorbent (g). The obtained results were fitted to non-linear kinetic models of general order, pseudo-first order and pseudo-second order.

$$Qe = \frac{(Ce - Cf) \times V}{m} \tag{1}$$

As for the equilibrium isotherms, 8 mg of adsorbent was kept in contact with 5 mL of PCM at 50, 100, 250, 500, 1,000, 1,500 and 2000 mg L^{-1} concentrations. After 5 h, the final drug concentration in the solution was determined. The adsorptive capacity was determined from Equation (1), and the data were fitted to the non-linear isothermal models of Langmuir, Freundlich and Sips.

All experiments were conducted at an ambient temperature of approximately 25 C, with constant stirring at 150 rpm. Solution concentrations were determined using a Kasuaki IL-593-S UV-Vis spectrophotometer at a wavelength of 242 nm. All experiments were performed in triplicates.

3 Computational model and details

3.1 *Ab initio* simulations

The *ab initio* simulation was performed using SIESTA code (Soler et al., 2002). They were evaluated through first-principles calculations based on DFT (Hohenberg and Kohn, 1964; Kohn and Sham, 1965) to obtain electronic, structural, and energetic properties. In all calculations, we used the local density approximation (LDA) parameterized by Perdew and Zunger to describe the exchange–correlation potential. LDA is more suitable than the Generalized Gradient Approximation (GGA) to study weakly interacting systems and also the presence of π-stacking interactions on sp^2-like materials. It is also important to outline that similar LDA calculations have been employed successfully in our group to describe the most diverse types of systems related to Gr-molecule interactions, resulting in an excellent tool for the connection between theory and experiments. Additionally, the present methodology used in this work allowed us for a feasible comparison with previously published work by our team, where the LDA results for binding energy and bond distance are very close to the experimental one (Jauris et al., 2017; de Oliveira et al., 2021; Bruckmann et al., 2022; Leão et al., 2023).

The interactions between the core and the valence electrons were employed through Troullier–Martins pseudopotentials (Troullier and Martins, 1991), whereas the molecular orbitals made use of a localized double zeta plus polarization (DZP) (Sankey and Niklewski, 1989) basis

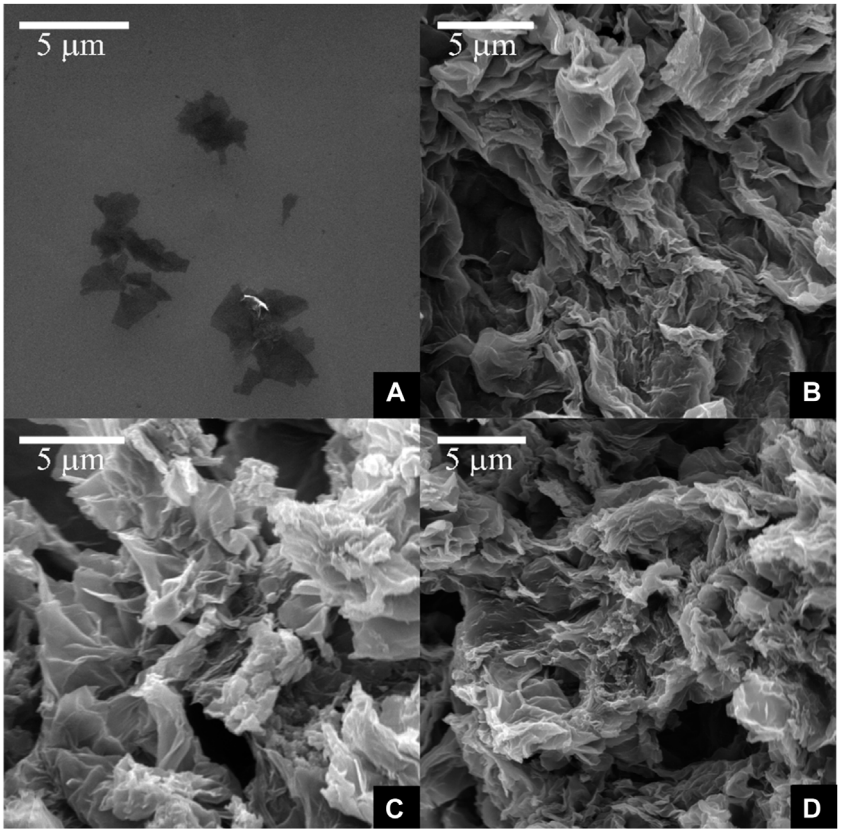

FIGURE 1
Scanning Electron Microscopy of 2D-rGO **(A)**, 3D-rGO0 **(B)**, 3D-rGO5 **(C)**, and 3D-rGO25 **(D)** materials.

TABLE 1 Properties of the materials obtained according to the characterizations performed (Leão et al., 2022).

Material	Concentration of COOH (mmol g^{-1})	Specific surface area (m^2 g^{-1})
2D-rGO	-	91.6
3D-rGO0	10.62 ± 1.84	172.274
3D-rGO5	3.08 ± 0.12	163.198
3D-rGO25	2.52 ± 1.34	62.807

set through a limited energy shift of 0.05 eV. The cutoff of 200 Ry in the grid integration represents the charge density for all interactions. Mulliken population analysis evaluated the electronic charge transfer between paracetamol (PCM) and graphene (Gr).

The structural optimization was performed by a conjugate gradient method. All atomic coordinates were allowed to move until the residual forces were less than 0.05 eV/Å. The computational method and simulation parameters were similar to those used in our previous work (de Oliveira et al., 2021; Bruckmann et al., 2022; Leão et al., 2023). These structures can describe qualitatively the results by combining simulations and experimental data for molecule adsorption.

Thus, the structures studied were graphene functionalized with one epoxy/two epoxy groups (Gr[O]/Gr[2O]), one hydroxyl/two hydroxyl groups (Gr[OH]/Gr[2OH]), and one carboxyl/two carboxyl groups (Gr[COOH]/Gr[2COOH]), where each of them interacts with PCM (CAS 103-90-2; $C_8H_9NO_2$). Three different pairs Gr[O]/Gr[2O], Gr[OH]/Gr[2OH], and Gr[COOH]/Gr[2COOH], were used in the simulation and represent the type and quantity of functional groups in the graphene model used. They reflect possible functional groups present in reduced graphene oxide structures. We do not use the same functional groups simultaneously, so it would be possible to evaluate their individual collaboration. These models were chosen to explain the effect of the type and quantity of functional groups on the PCM adsorption mechanism on three-dimensional materials based on graphene, whose structural differences are mainly due to the amount and kind of oxygenated groups.

The optimized structures can be seen in Supplementary Figure S1. We use several different configurations for every system associated with PCM. Notably, only the most stable configurations are presented in this work. The final binding energies (EB) were calculated according to Equation 2, which is based on the Basis Set Superposition Error (BSSE) (Boys and Bernardi, 1970),

$$EB = -\left[E(Gr + PCM) - E(Grghost + PCM) - E(Gr + PCMghost)\right] \quad (2)$$

where EB is the binding energy, EB(Gr + PCM) is the total energy of the Gr plus PCM molecule. The subscript "ghost" corresponds to the additional basis wave functions centered at the position of the Gr or at the PCM molecule but without any atomic potential. The minimum distance (DB) values between the PCM and the Gr

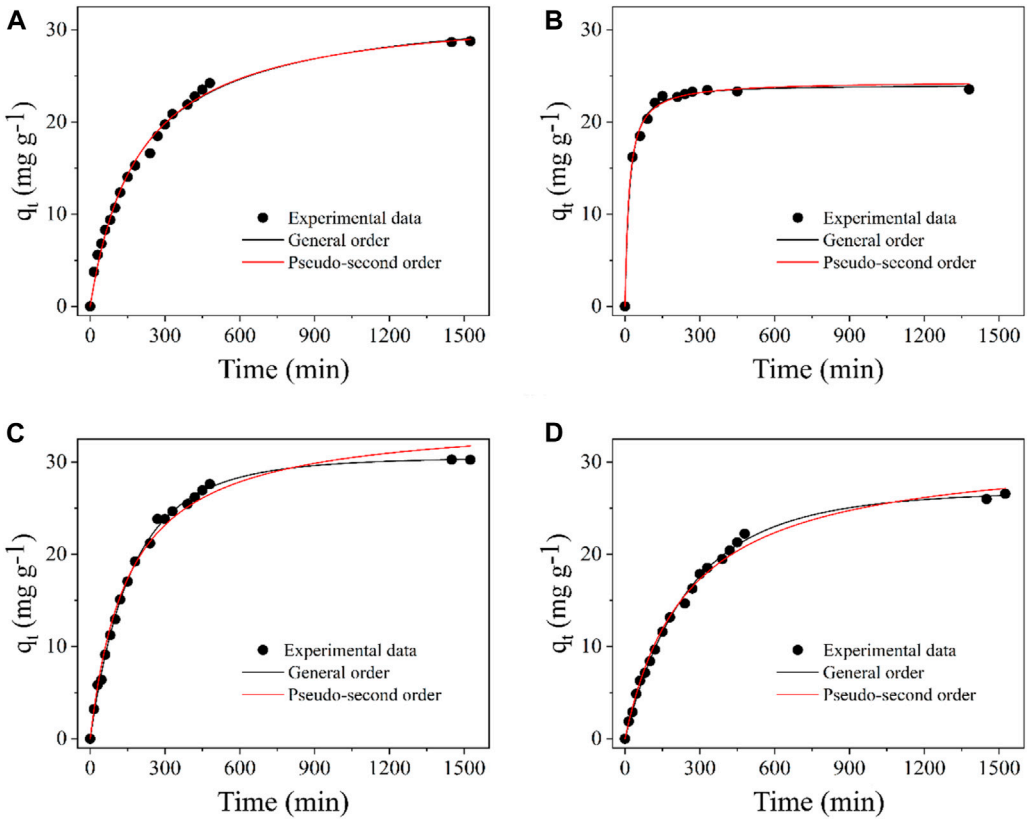

FIGURE 2
Adsorption kinetics of paracetamol in 2D-rGO **(A)**, 3D-rGO0 **(B)**; 3D-rGO5 **(C)**, and 3D-rGO25 **(D)**.

TABLE 2 The kinetic parameters for paracetamol adsorption by 2D-rGO, 3D-rGO0, 3D-rGO5, and 3D-rGO25.

	2D-rGO	3D-rGO0	3D-rGO5	3D-rGO25
General-order				
k_N(min^{-1}.(g.mg^{-1})$^{n-1}$)	9.46 × 10^{-5}	0.005	0.003	0.002
q_e (mg.g^{-1})	33.529	23,998	30,517	26,938
n	2.140	1,770	1,233	1,213
$t_{1/2}$ (min)	203,829	16,693	123,602	188,380
R^2_{adj}	0.9925	0.9949	0.9978	0.9973
SD	0.719	0.476	0.447	0.420
Pseudo-second order				
k_2(g.mg^{-1}.min^{-1})	1.590 × 10^{-4}	0.003	1,886 × 10^{-4}	1,282 × 10^{-4}
q_e (mg.g^{-1})	32.634	24,417	34,902	31,544
$t_{1/2}$ (min)	192,728	15,910	151,871	247,299
R^2_{adj}	0.9930	0.9950	0.9911	0.9937
SD	0.7013	0.474	0.8956	0.642

were obtained from the nearest atoms. The bond distance (DB) values between PCM and Gr are obtained from the minimum interatomic distance between the systems. In this paper, to quantify an interaction such as physical or chemical adsorption, we considered parameters such as charge transfer, bond distance, and detailed analysis from the electronic energy levels of the systems, similar to those used in previous works (Vendrame et al., 2019; Concu et al., 2020; Leão et al., 2022; Leão et al., 2023).

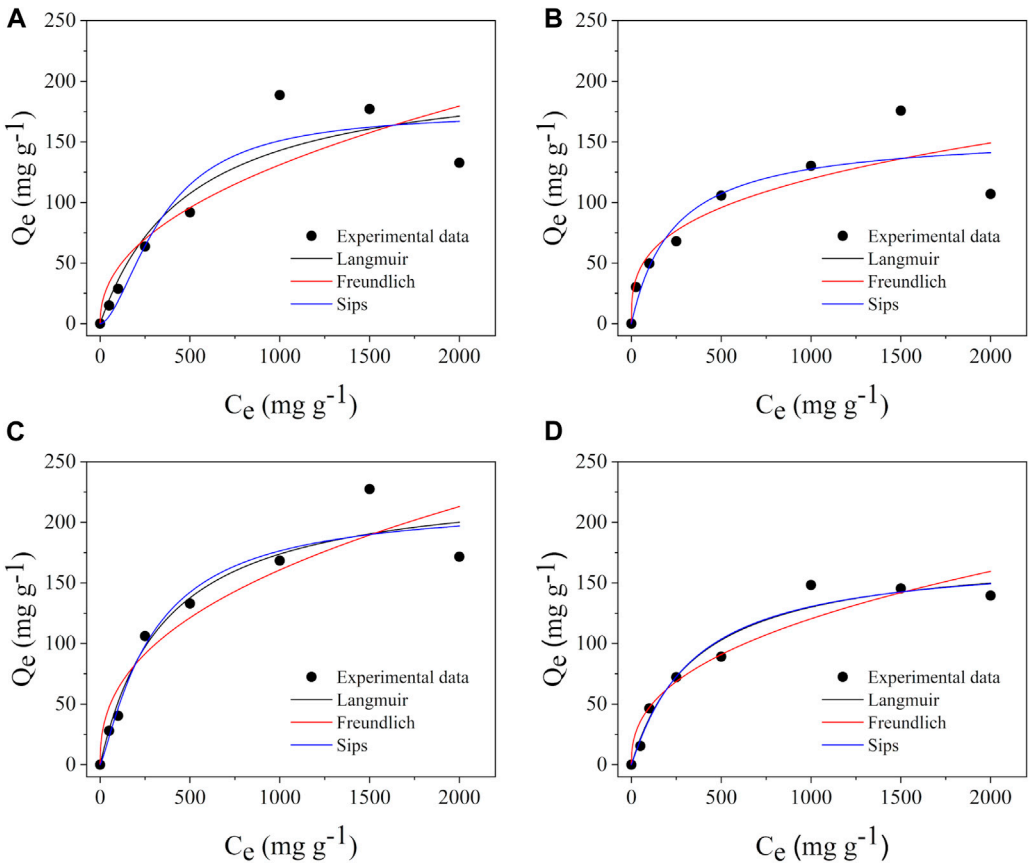

FIGURE 3
Adsorption isotherms of paracetamol in 2D-rGO **(A)**, 3D-rGO0 **(B)**; 3D-rGO5 **(C)**, and 3D-rGO25 **(D)**.

4 Results and discussion

4.1 Material characterization

As already mentioned, a detailed version of the characterization of these materials can be found in the article that describes the process of synthesis and characterization of these materials (Leão et al., 2022). The SEM images of the four studied materials are shown in Figure 1. The structural difference between 2D-rGO (Figure 1A) and 3D materials can be observed. While the first one appears as small sheets, the others have these sheets interconnected disorderly, forming a three-dimensional porous network. It is also possible to observe significant differences among the 3D materials (Figure 1B–D). The greater the amount of reducing agent added, the greater the compaction of the structure, which has smaller cavities. Thus, it can be expected that different behaviors are found for the materials due to their morphology. Self-assembling graphene oxide sheets form 3D graphene network structures through hydrogen bonding, electrostatic interaction, or π-π interactions. Wang et al. (2019) Considering the self-assembly mechanism of graphene hydrogels via hydrothermal routes, the pore size results from the size of the bubbles formed during the process. It must be considered that a greater degree of oxygen functionalization promotes greater interaction with the polar solvent, leaving larger hydrate pores. However, when the reduction process removes the hydrophilic groups, the water in the pore decreases, consequently allowing for higher structure compaction.

The results of the concentration of functional groups (Table 1) show that the greater the amount of reducing agent added, the smaller the number of oxygenated groups. These results are corroborated by the FTIR spectra available in (Leão et al., 2022). Likewise, for 3D materials, the greater the amount of reducing agent, the smaller the material-specific surface areas; the 2D-rGO material has an intermediate surface, closer to the 3D-rGO25 material–which is the 3D version closest to it. The combination of these results shows that the variation in the amount of reducing agent used interferes with the chemical structure and the morphology of the materials.

4.2 Experimental adsorption results

From the experimental adsorption studies, it was possible to compare the efficiencies of the materials as follows. The kinetic study, shown in Figure 2, and detailed data in Table 2, show that the behavior of the adsorption rate is influenced by the synthesis method and the concentration of the reducing agent, that is, the presence of functional groups. Reaching adsorption equilibrium was approximately 5 h for 3D-rGO0, 12 h for 3D-rGO5, 20 h for 3D-rGO25 and 24 h for 2D-rGO. Respectively, for the four materials, $t_{1/2}$ was 15.9, 123.6, 188.4 and 192.7 min. This last value represents the

TABLE 3 Isotherm parameters for paracetamol adsorption using 2D-rGO, 3D-rGO0, 3D-rGO5 and 3D-rGO25 adsorbent.

	2D-rGO	3D-rGO0	3D-rGO5	3D-rGO25
Langmuir				
Q_{max} ($mg.g^{-1}$)	213,48	157,647	235,692	176,765
K_L ($L.mg^{-1}$)	0.0020	0.0043	0.0028	0.0028
R^2_{adj}	0,8677	0,8404	0,9372	0,9647
SD	26,531	22,869	20,140	11,067
Freundlich				
K_F ($mg.g^{-1}(mg.L^{-1})^{-1/n_F}$)	5,703	13,148	9,685	7,291
n_F	2,204	3,130	2,459	2,463
R^2_{adj}	0.7937	0.8095	0.8850	0.9226
SD	33,136	24,986	27,244	16,394
Sips				
Q_{max} ($mg.g^{-1}$)	175,098	157,647	215,902	172,335
K_s ($L.mg^{-1}$)	$4,431 \times 10^{-5}$	0.004	0.001	0.002
n_s	0.583	1	0.827	0.953
R^2_{adj}	0.8678	0.8085	0.9280	0.9579
SD	26,528	25,051	21,562	12,091

TABLE 4 Binding distance (DB), charge transfer [△q (e–)], Highest Occupied Molecular Orbital (HOMO), Lowest Unoccupied Molecular Orbital (LUMO) difference (△HL), and binding Q21 energy (EB). The positive signal in the charge transfer indicates that the Gr is a charge donor. The bold values correspond to the most stable structures.

Configuration	DB (Å)	Δq (e–)	ΔHL (eV)	EB (eV)
Gr[O]+PCM-I	2.33 (OGr-HPCM)	0.21	1.34	0.38
Gr[O]+PCM-II	**1.88 (OGr-HPCM)**	**0.29**	**1.25**	**0.60**
Gr[O]+PCM-III	2.29 (OGr-HPCM)	0.16	1.50	0.23
Gr[2O]+PCM-I	2.16 (OGr-HPCM)	0.13	1.56	0.27
Gr[2O]+PCM-II	**2.00 (OGr-HPCM)**	**0.35**	**1.31**	**0.49**
Gr[2O]+PCM-III	2.13 (OGr-HPCM)	0.05	1.55	0.24

time required for 50% of the analyte to be adsorbed and is used to compare the different materials (Thue et al., 2018).

From these results, we can infer that the 3D-rGO0 material can adsorb PCM faster, followed by the 3D-rGO5, 3D-rGO25, and 2D-rGO materials. Similar behavior has been described previously in our articles (Vijayaraghavan et al., 2006; Leão et al., 2022) in the adsorption of safranin and methylene blue dyes. We verified, then, that the behavior obtained for the dyes can be extended to the drug PCM. As in previous works, adsorption takes place more quickly in materials where there is a greater amount of oxygenated functional groups and the presence of larger cavities and/or pores. Additionally, the 3D-rGO0 material presents different behavior due to its granular structure. This structural configuration allows a larger material area to interact with the PCM, accelerating the adsorptive process. In the case of other materials, the intra-particle diffusion process must be responsible for the increased velocity in materials with larger pore sizes. As seen previously, the greater the amount of reducing agent added during synthesis, the smaller the cavities/pores, and the more compact the structure. At the same time, smaller amounts of oxygenated functional groups are available for interaction with the analytes. Such conditions guarantee the order of adsorption speed in the studied materials.

Adsorption isotherms were constructed to determine the adsorptive capacity of the materials for the drug PCM (Figure 3). The adsorptive capacities of 235.7, 176.8, 175.1 and 157.6 mg g^{-1} were determined for 3D-rGO5, 3D-rGO25, 2D-rGO, and 3D-rGO0 materials, respectively (Table 3). An important observation point is the isothermal models that best fit each result. While all three three-dimensional materials showed a better fit to the Langmuir isothermal model, only 2D-rGO showed a better fit to the Sips isothermal model. This result indicates that their dimensionality influences the adsorptive behavior of the materials. While the Langmuir model

10.3389/frcrb.2024.1305183

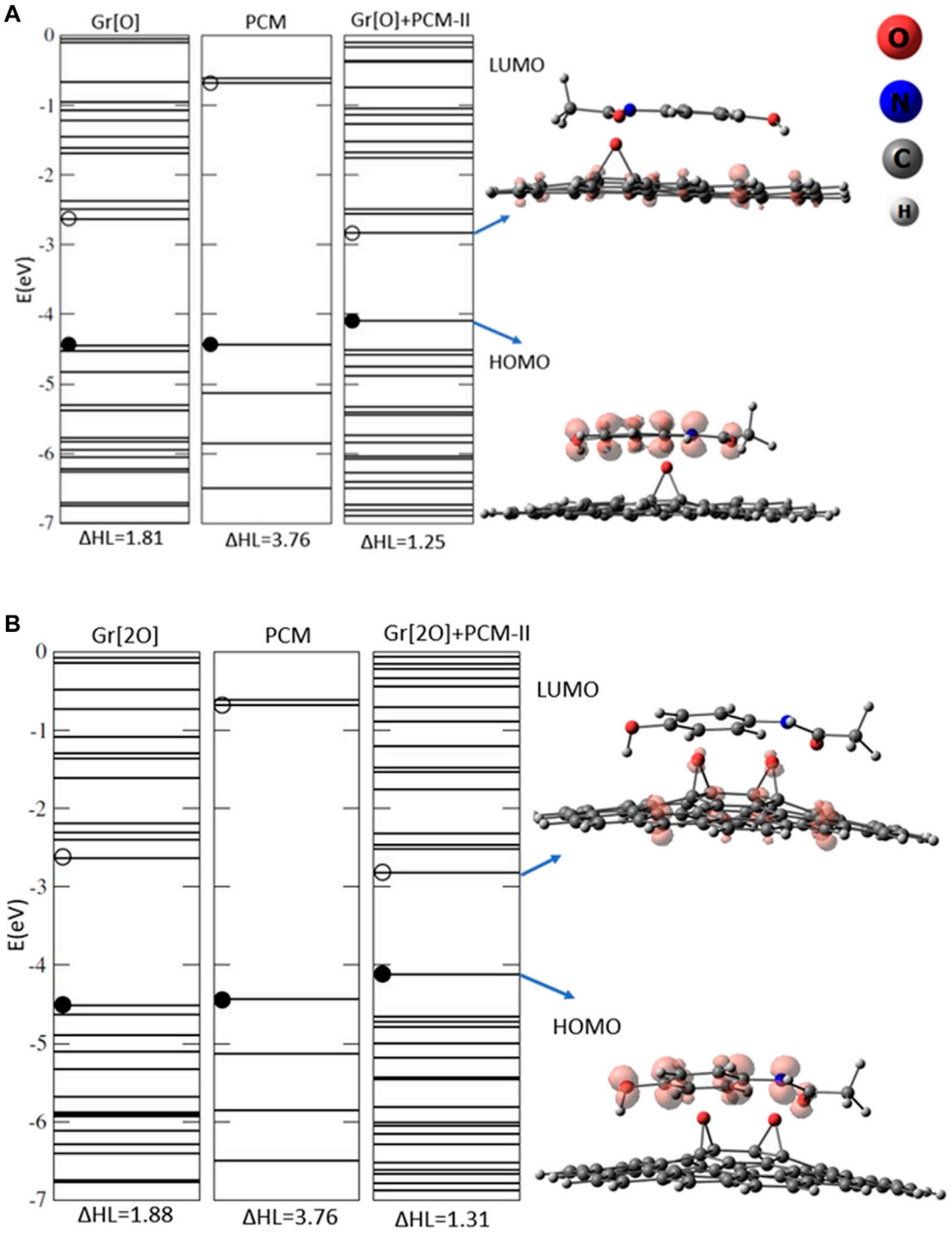

FIGURE 4
Electronic levels and LDOS for the most stable configuration: **(A)** Gr[O] +PCM-II and **(B)** Gr[2O]+PCM-II configurations with orbital charge density isosurfaces 0.0093 e−/(Å)^3.

describes monolayer adsorption, the Sips model, also called Langmuir-Freundlich, has two behaviors: at low adsorbate concentrations, it reduces to the Freundlich isotherm (Vijayaraghavan et al., 2006), and at high concentrations, predicts monolayer adsorption, with a limited number of sites on the surface of the adsorbent, characteristic of the Langmuir isotherm (Lima et al., 2015; Soltani et al., 2019).

Another important point in the adsorption study concerns the differences in adsorption capacities. Differently from the kinetic study, there is a highlight for the 3D-rGO5 material, which can absorb 235.7 mg g^{-1}. Next, we observed that the 3D-rGO25 and 2D-rGO materials have similar adsorptive capacities. In common, both materials have the highest addition of reducing agent (25 mmol L^{-1}), presenting a similar degree of reduction. Finally, the 3D-rGO0

10.3389/frcrb.2024.1305183

TABLE 5 Relevant data for minimum distance (DB), charge transfer (Δq (e–)), HOMO and LUMO difference (ΔHL), and binding energy (EB). The positive signal in the charge transfer indicates that the oxidized graphene is a charge donor.

Configuration	DB (Å)	Δq (e–)	ΔHL (eV)	EB(eV)
Gr[OH]+PCM-I	2.37 (CGr-HPCM)	0.17	1.72	0.30
Gr[OH]+PCM-II	2.37 (CGr-HPCM)	0.19	1.64	0.35
Gr[OH]+PCM-III	**1.75 (HGr-OPCM)**	0	**1.80**	**0.60**
Gr[2OH]+PCM-I	1.92 (OGr-HPCM)	0.13	1.12	0.47
Gr[2OH]+PCM-II	1.76 (OGr-HPCM)	0.35	0.66	0.69
Gr[2OH]+PCM-III	**1.52 (HGr-OPCM)**	**0.05**	**1.13**	**1.28**

material, which has excellent kinetic performance, has the lowest adsorptive capacity. From these results, we can infer some considerations. First, material morphology appears to be dominant in the adsorptive process. This can be observed mainly for the 3D-rGO0 material, which can adsorb PCM quickly but not in large quantities due to its loose granular structure. Secondly, due to similar synthesis, 3D-rGO25 and 2D-rGO materials have identical amounts of oxygenated groups. Thus, it can be deduced that smaller amounts of oxygenated functional groups result in smaller quantities of PCM. The presence of oxygenated groups is a secondary factor in the adsorption. Finally, 3D-rGO5 stands out, which presents a cohesive three-dimensional structure, is porous, less compacted, and has larger cavities and an intermediate number of oxygenated groups. Such material seems ideal for the adsorption of the drug PCM, due to its morphology and presence of oxygenated groups.

4.3 Computational results

Theoretical calculations were conducted to understand the interaction mechanisms between different three-dimensional graphene materials and the drug paracetamol, focusing on the type and number of oxygenated groups in the materials. This section provides the details of the calculations.

4.3.1 Ab initio simulations - Gr[O]/Gr[2O] interacting with PCM

To gain insights into the atomistic details of the interaction, we present the main results for Gr[O] and Gr[2O], graphene with one and two oxygen atoms attached, respectively. Both interact with the PCM molecule, and the results for the most stable configurations are presented in Table 4. The optimized structures of the most stable configurations can be found in the Supplementary Figure S2.

Table 1 presents the minimum atomic distance (DB), binding energy (EB) and electronic charge transfer (Δq (e–)) of the most stable configurations for both Gr[O]+PCM and Gr[2O]+PCM systems.

All results showed that these systems interact in a physisorption regime for both Gr structures. For PCM adsorbed on Gr[O], the most stable configuration was Gr[O]+PCM-II, with a binding energy of 0.60 eV and a distance of 1.88 Å (OGr-HPCM). The same occurs to PCM adsorbed on Gr[2O]. The most stable configuration was Gr[2O] + PCM-II, where this system presents a 0.49 eV for the binding energy with a binding distance of 2.00 Å (OGr-HPCM).

In the binding distance column, the first atom always refers to a graphene (Gr) atomic structure, while the second refers to a paracetamol (PCM) molecule. Figure 4 shows the energy levels for the Gr[O]+PCM-II and Gr[2O] + PCM-II systems. The same figure also presents the local density of states (LDOS) for the HOMO and LUMO levels.

The difference between the highest occupied molecular orbital (HOMO, represented by the solid black circle) and the lowest unoccupied molecular orbital (LUMO, represented by the hollow circle) is given in electron volts (eV). The values found are 1.81 eV for isolated graphene with one oxygen atom (Gr[O]) and 1.25 eV for the most stable interacting system between these two structures (Gr[O]+PCM-II). For isolated graphene with two oxygen atoms (Gr[2O]), the difference between HOMO and LUMO is 1.88 eV, and the interacting system, Gr[2O]+PCM-II, shows a value of 1.31 eV.

The difference between HOMO and LUMO levels is similar to the isolated graphene, without significant changes. Furthermore, we observe that there is only an overlap of the paracetamol (PCM) molecule levels with the graphene but no substantial changes in the electronic properties of the resultant system compared to the pristine ones.

Regarding the local density of states (LDOS) analysis, both systems, with one or two oxygen atoms attached to graphene, show HOMO energy level contribution on the PCM molecule, while the LUMO on the graphene structure. This characteristic leads us to a physisorption mechanism since we have only one structure contribution for each energy level.

4.3.2 *Ab initio* simulations - Gr[OH]/Gr[2OH] interacting with PCM

Here, we show Gr[OH] and Gr[2OH] data. This means we now considered two different types of oxidized Gr: the first has one OH chemical group, and the second has two OH chemical groups attached to its surface.

Both Gr[OH] and Gr[2OH] interact with PCM molecules in multiple configurations, and the key data are presented in Table 5. Table 5 shows the minimum atomic distance (DB), binding energy (EB), and electronic charge transfer (Δq (e–)) of the most stable configurations for both the Gr[OH]+PCM and Gr[2OH]+PCM systems. The optimized structures of the most stable configurations can be seen in the Supplementary Figure S3.

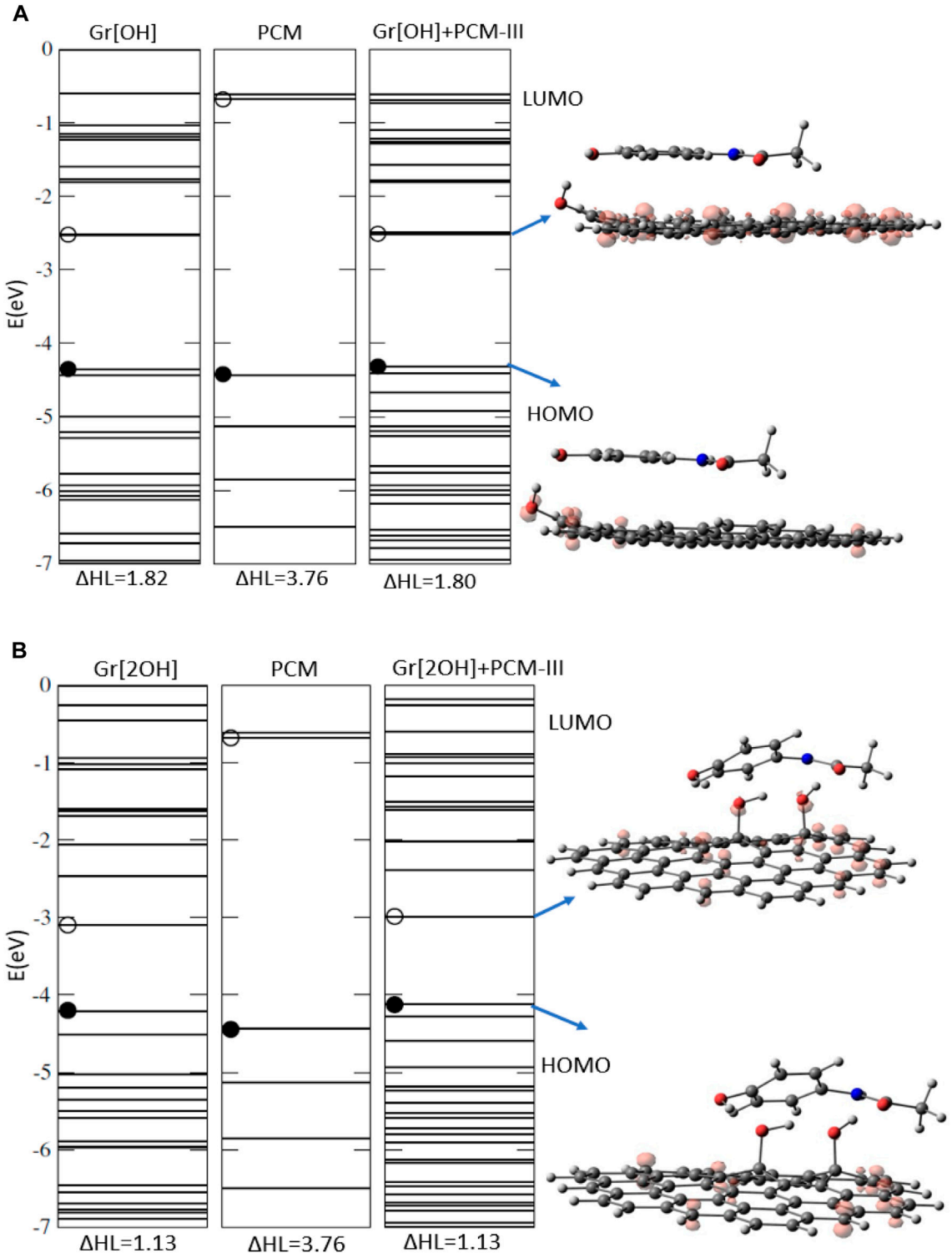

FIGURE 5
Electronic levels and LDOS for the most stable configuration: **(A)** Gr[OH] interacting with PCM (Gr[OH]+PCM-III) and **(B)** Gr[2OH] interacting with PCM molecule (Gr[2OH]+PCM-III) with orbital charge density isosurfaces 0.0093 e–/(Å)^3.

For PCM adsorbed on Gr[OH], the most stable configuration was Gr[OH]+PCM-III, with a binding energy of 0.60 eV and a distance of 1.75 Å (HGr-OPCM). For PCM adsorbed on Gr[2OH], the most stable configuration was Gr[2OH]+PCM-III, where this system presents a 1.28 eV for the binding energy with a binding distance of 1.52 Å (HGr-OPCM).

The binding energies for Gr[2OH]+PCM-III are high, suggesting the possibility of chemical interaction. However, the bond distance and

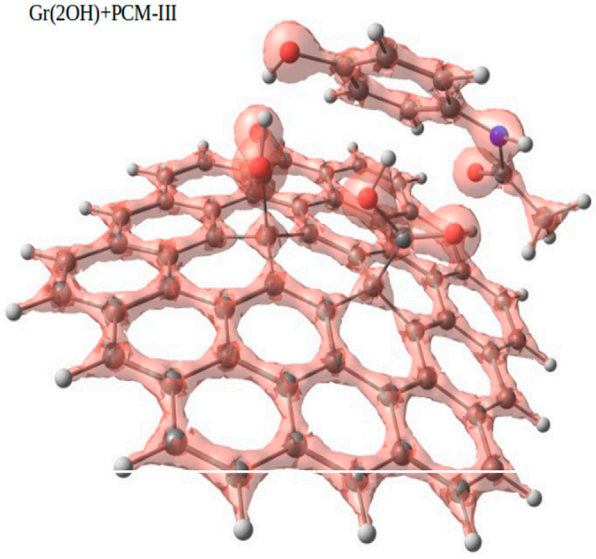

FIGURE 6
Total electronic charge density isosurface for the most stable configurations for Gr[2OH]+PCM-III using orbital charge density isosurfaces of 0.0093 e–/(Å)^3.

charge transfer values for Gr[2OH]+PCM-III are incompatible with chemisorption. Therefore, the presence of these hydrogen bonds cannot lead to significant changes in the physical adsorption regime of PCM on graphene. An electronic study of these configurations was conducted to confirm these findings, and the results are shown in Figure 5 and Figure 6.

Figure 5 shows the energy levels and the local density of states (LDOS) for both the Gr[OH]+PCM-III and Gr[2OH]+PCM-III systems. We can see that the HOMO energy level has a contribution from the graphene (Gr) structure, and the same occurs with the LUMO. This data suggests that both systems are interacting through the physisorption regime. However, the system with two OH chemical groups has a smaller binding distance and higher binding energy. For a more detailed analysis, Figure 6 shows the total charge density isosurface plots for the most stable configuration, Gr[2OH]+PCM-III, to investigate the possibility of chemisorption.

This analysis scans every single energy level of the system and shows its total electronic distribution, allowing us to confirm whether there is chemisorption between the structures (Figure 6). The image confirms no chemisorption between the -OH chemical groups and the PCM molecule. As can be seen, the charges are localized only on the Gr(2OH) and PCM molecules, with no charge lines shared between the systems. There is no electron sharing between the two structures. This result confirms that this system exhibits a physisorption interaction, as observed in previous work with graphene nanomaterials and different molecules (de Oliveira et al., 2021; Bruckmann et al., 2022; Leão et al., 2023).

4.3.3 *Ab initio* simulations - Gr[COOH]/Gr[2COOH] interacting with PCM

At last, we present the data for Gr[COOH] and Gr[2COOH]. In this case, we now have a first Gr with one COOH chemical group and a second Gr with two COOH chemical groups attached to their surface. Both Grs interact with the PCM molecule. Table 6 presents the minimum atomic distance (DB), binding energy (EB), and electronic charge transfer (Δq(e–)) of the most stable configurations for both Gr[COOH]+PCM and Gr[2COOH]+PCM systems. The optimized structures of the most stable configurations can be seen in Supplementary Figure S4.

The binding energy features the configuration Gr[COOH]+PCM-II and Gr[2COOH]+PCM-III as the most stable for Gr[COOH]+PCM and Gr[2COOH]+PCM systems, respectively. After calculating the BSSE, we found a 0.79 eV and DB of 1.61 Å (OGr-HPCM) for Gr[COOH]+PCM-II and 1.48 eV and DB of 1.49 Å (OGr-HPCM) for Gr[2COOH]+PCM-III systems. Figure 7 shows the energy levels and the LDOS for both Gr[COOH]+PCM-II and Gr[2COOH]+PCM-III systems.

We can observe that the HOMO energy level shows a contribution from the PCM molecule for the Gr[COOH]+PCM-II system and a contribution from the Gr[COOH] structure for the Gr[COOH]+PCM-III system. In the LUMO level, we can observe a contribution from Gr[2COOH] with a strong contribution from the functionalized COOH groups.

The binding energies for Gr[2COOH]+PCM-II and Gr[2COOH]+PCM-III are high, as we also observed for Gr[2OH]+PCM-II, suggesting the existence of chemical interaction. It is important to emphasize that in both cases, more than one functional group in the Gr increases the interactions with the PCM molecule. Once again, we performed the total electronic charge density isosurface analysis to check for any signs of chemisorption for the Gr[2COOH]+PCM-II and Gr[2COOH]+PCM-III systems, shown in Figure 8.

TABLE 6 Binding distance (DB), charge transfer (Δq (e–)), HOMO and LUMO difference (ΔHL), and binding energy (EB). The positive signal in the charge transfer indicates that the graphene is a charge donor.

Configurations	DB (Å)	Δq (e–)	ΔHL (eV)	EB (eV)
Gr[COOH]+PCM-I	2.22 (OGr-HPCM)	0.15	1.54	0.34
Gr[COOH]+PCM-II	**1.61 (OGr-HPCM)**	**0.32**	**1.18**	**0.79**
Gr[COOH]+PCM-III	2.81 (CGr-HPCM)	0.12	1.43	0.12
Gr[2COOH]+PCM-I	1.66 (OGr-HPCM)	0.38	1.25	0.63
Gr[2COOH]+PCM-II	1.41 (HGr-OPCM)	0.01	1.75	1.26
Gr[2COOH]+PCM-III	**1.49 (OGr-HPCM)**	**0.13**	**1.81**	**1.48**

10.3389/frcrb.2024.1305183

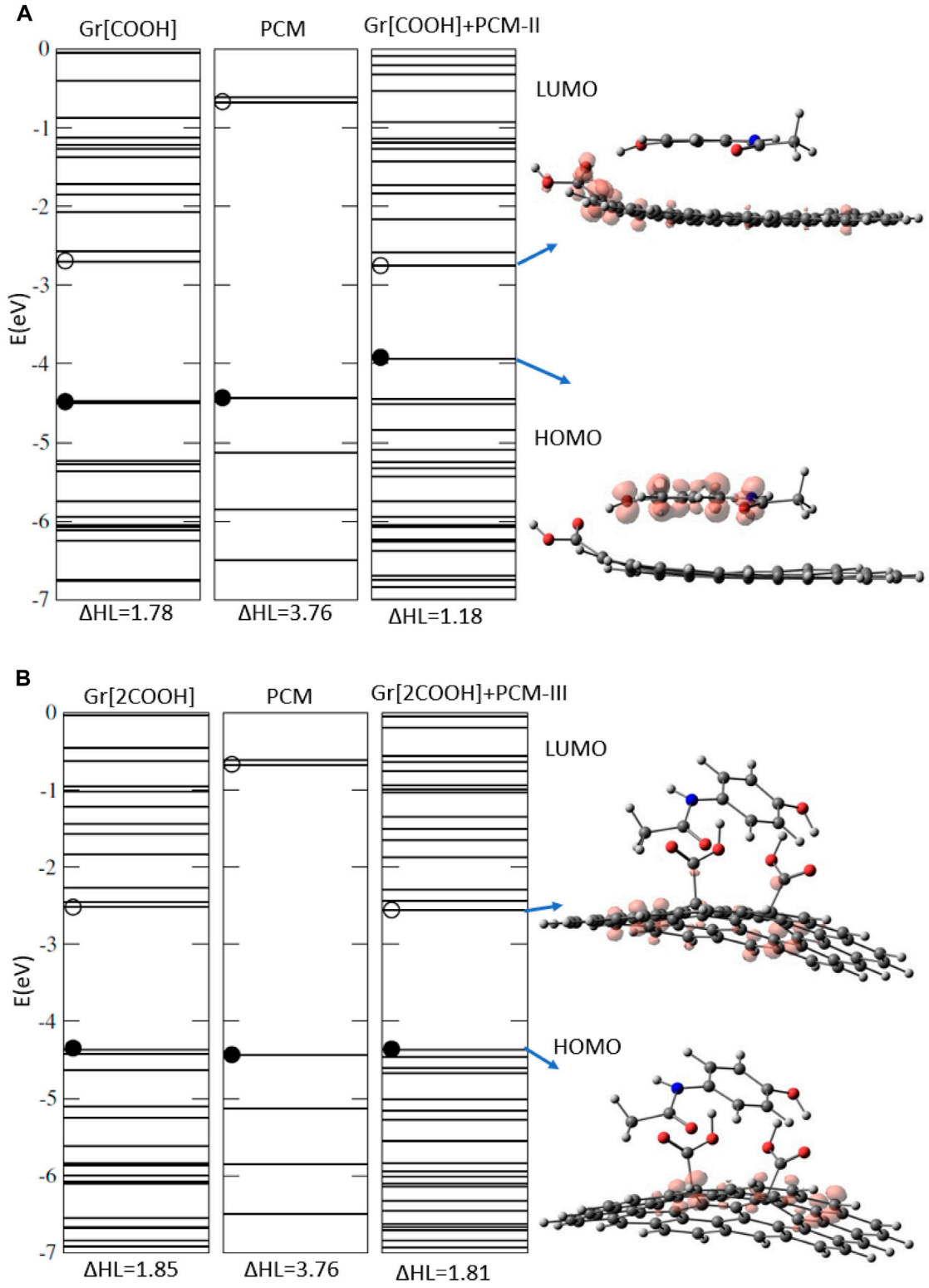

FIGURE 7
Electronic levels and LDOS for the most stable configuration of **(A)** Gr[COOH] interacting with PCM (Gr[COOH]+PCM-II), **(B)** Gr[2COOH] interacting with PCM molecule (Gr[2COOH]+PCM-III) with orbital charge density isosurfaces 0.0093 e–/(Å)^3.

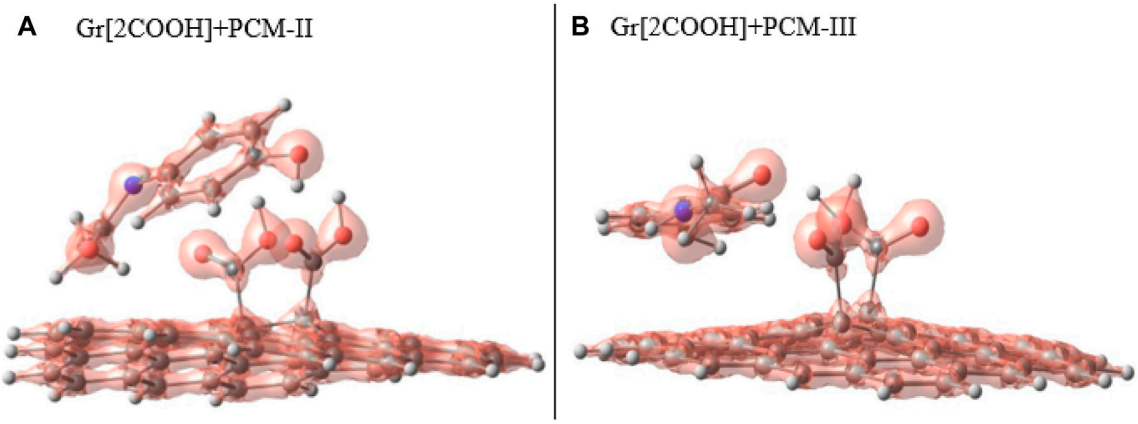

FIGURE 8
Total electronic charge density isosurface for the most stable configurations for **(A)** Gr[2COOH]+PCM-II, **(B)** Gr[2COOH]+PCM-III using orbital charge density isosurfaces of 0.0093 e−/(Å)3.

In Figure 8A, it is made clear that the PCM molecule does not share electrons with anyone close to it, and in Figure 8B, we can also confirm that the Gr structure and PCM molecule cannot share electrons with how they are arranged.

Despite the high binding energies and/or small binding distances observed for the Gr[2OH] and Gr[2COOH] systems, all systems exhibited a physisorption regime. This suggests that increasing the number of functional groups tends to increase the energies and binding of the systems.

The adsorption of PCM onto graphene, with one or two functionalizations, was simulated to provide a good understanding of the adsorption process of the PCM molecule onto the surfaces of functionalized graphene materials. The Mulliken population analysis showed that the electronic charge transfers indicate that graphene materials have an amphoteric character, depending on the position of the PCM during the adsorption process.

In addition to the binding energies, the high values of the minimum distance between the systems, the low values of charge transfer, and the total charge density between the systems indicate that the interaction occurred through a physical adsorption regime. A strong hydrogen bonding tendency was observed between the functional groups and PCM for all functional groups attached to graphene, increasing the number of epoxy, hydroxyl, and carboxyl functional groups on the graphene surface led to significant increases in the graphene+PCM binding energy. Therefore, the intensity of the binding energies depends on the presence of some types of functional groups on the graphene surface. A deformation in the Gr structure is also observed as the number of functionalized groups increases. These results agree with the experimental data, where the highest adsorptions were observed for materials containing a higher proportion of functional groups and where these groups are more available, such as the 3D-rGO5 material. Our research group also found similar results in recent works with methylene blue (Leão et al., 2023). The three different functional groups attached to the graphene surface used in the simulation reflect the 2D-rGO experimental synthesized well. The results from graphene Gr[OH]/Gr[2OH] and Gr[COOH]/Gr[2COOH] are consistent, showing that increasing the number of functional groups leads to an increase in binding energies. Greater binding energy can also be associated with a better adsorption capacity. As described in experimental results, due to similar synthesis, 3D-rGO25 and 2D-rGO materials have identical amounts of oxygenated groups. Regardless of 3D-rGO25 pursuit cavities/pores in comparison with 2D-rGO, which are more compact structures, it can be noted that the adsorption capacities were similar in both cases; thus, the number of functional groups could be responsible for these similarities. On the other hand, 3D-rGO5, which presents a structure similar to 3D-rGO25, exhibits better adsorption compacity than 3D-rGO25, revealing that more functional groups could enhance the adsorption capacity up to a threshold.

5 Conclusion

Our results showed that three-dimensional graphene-based materials exhibit interesting adsorption results with only minor changes in the material synthesis. These changes result in variations in the specific surface areas, pore sizes, and amount of oxygenated functional groups in the structure. The combination of experiments with computational studies allowed us to verify the influence of these characteristics of the materials on the adsorption of paracetamol.

Generally, it was observed that the more oxidized the material, the greater the adsorption efficiency, except for the material without adding a reducing agent, which does not form a three-dimensional porous structure. Ab initio studies revealed that the binding energies, bond distances, and charge transfer between oxidized graphene and the PCM drug are compatible with physical adsorption. The results demonstrate no chemisorption, as confirmed by the total electronic charge density measure. Moreover, the intensity of physical adsorption strongly depends on the type of oxygen group on the graphene surface, increasing as the number of functional groups increases. These results satisfactorily explain the results obtained experimentally: the larger the pores (which makes it easier for paracetamol to reach oxygenated sites), the more oxidized the material, and the better its efficiency in adsorbing paracetamol.

Data availability statement

The original contributions presented in the study are included in the article/Supplementary material, further inquiries can be directed to the corresponding author.

Author contributions

CM: Data curation, Investigation, Writing–original draft. ML: Data curation, Investigation, Writing–original draft. LV: Formal Analysis, Methodology, Software, Writing–original draft. IJ: Formal Analysis, Methodology, Software, Writing–original draft. IZ: Conceptualization, Software, Supervision, Validation, Writing–review and editing. SF: Conceptualization, Funding acquisition, Resources, Supervision, Validation, Writing–review and editing.

Funding

The author(s) declare that financial support was received for the research, authorship, and/or publication of this article. The author(s) declare that receive financial support from Brazilian National Council for Scientific and Technological Development (CNPq, proc. 424146/2018- 5 and proc. 403427/2021-5), Coordination for the Improvement of Higher Education Personnel (CAPES, financing Code 001), Research Support Foundation of the State of Rio Grande do Sul (FAPERGS, TO 21/2551-0000736-2 and TO 21/2551-0002024-5).

Conflict of interest

The authors declare that the research was conducted in the absence of any commercial or financial relationships that could be construed as a potential conflict of interest.

Publisher's note

All claims expressed in this article are solely those of the authors and do not necessarily represent those of their affiliated organizations, or those of the publisher, the editors and the reviewers. Any product that may be evaluated in this article, or claim that may be made by its manufacturer, is not guaranteed or endorsed by the publisher.

Supplementary material

The Supplementary Material for this article can be found online at: https://www.frontiersin.org/articles/10.3389/frcrb.2024.1305183/full#supplementary-material

References

Albert, O., Desdoits-Lethimonier, C., Lesné, L., Legrand, A., Guillé, F., Bensalah, K., et al. (2013). Paracetamol, aspirin and indomethacin display endocrine disrupting properties in the adult human testis *in vitro*. *Hum. Reprod.* 28, 1890–1898. doi:10.1093/humrep/det112

Alves, D. C. d.S., Healy, B., Yu, T., and Breslin, C. B. (2021). Graphene-based materials immobilized within chitosan: applications as adsorbents for the removal of aquatic pollutants. *Materials* 14, 3655. doi:10.3390/ma14133655

Bedner, M., and MacCrehan, W. A. (2006). Transformation of acetaminophen by chlorination produces the toxicants 1, 4-benzoquinone and N-acetyl-p-benzoquinone imine. *Environ. Sci. Technol.* 40, 516–522. doi:10.1021/es0509073

Bolisetty, S., Peydayesh, M., and Mezzenga, R. (2019). Sustainable technologies for water purification from heavy metals: review and analysis. *Chem. Soc. Rev.* 48, 463–487. doi:10.1039/c8cs00493e

Boys, S. F., and Bernardi, F. (1970). The calculation of small molecular interactions by the differences of separate total energies. Some procedures with reduced errors. *Mol. Phys.* 19, 553–566. doi:10.1080/00268977000101561

Bruckmann, F. d. S., Zuchetto, T., Ledur, C. M., dos Santos, C. L., da Silva, W. L., Binotto Fagan, S., et al. (2022). Methylphenidate adsorption onto graphene derivatives: theory and experiment. *New J. Chem.* 46, 4283–4291. doi:10.1039/d1nj03916d

Concu, R., González-Durruthy, M., Cordeiro, M. N. D., Zanela, I., and Cordeiro, D. (2020). Developing a multi-target model to predict the activity of monoamine oxidase A and B drugs. *Curr. Top. Med. Chem.* 20, 1593–1600. doi:10.2174/1568026620666200603121224

de Oliveira, P. V., Zanella, I., Bulhoes, L. O. S., and Fagan, S. B. (2021). Adsorption of 17 β-estradiol in graphene oxide through the competing methanol co-solvent: experimental and computational analysis. *J. Mol. Liq.* 321, 114738. doi:10.1016/j.molliq.2020.114738

Deshwal, N., Singh, M. B., Bahadur, I., Kaushik, N., Kaushik, N. K., Singh, P., et al. (2023). A review on recent advancements on removal of harmful metal/metal ions using graphene oxide: experimental and theoretical approaches. *Sci. Total Environ.* 858, 159672. doi:10.1016/j.scitotenv.2022.159672

Ersan, G., Apul, O. G., Perreault, F., and Karanfil, T. (2017). Adsorption of organic contaminants by graphene nanosheets: a review. *Water Res.* 126, 385–398. doi:10.1016/j.watres.2017.08.010

Fan, S., Yu, Z., Wang, X., Tao, Y., Shao, H., Long, M., et al. (2023). A facile graphene oxide modified approach towards membrane with prominent improved permeability and antifouling performance. *Desalination* 545, 116130. doi:10.1016/j.desal.2022.116130

Fernandez, M. E., Ledesma, B., Román, S., Bonelli, P. R., and Cukierman, A. L. (2015). Development and characterization of activated hydrochars from orange peels as potential adsorbents for emerging organic contaminants. *Bioresour. Technol.* 183, 221–228. doi:10.1016/j.biortech.2015.02.035

Guo, Z., Feng, Y., Zhang, C., Huang, G., Chi, J., Yao, Q., et al. (2021). Three dimensional graphene materials doped with heteroatoms for extraction and adsorption of environmental pollutants in wastewater. *J. Environ. Sci. Health, Part C* 39, 17–43. doi:10.1080/26896583.2020.1863725

Hamed, R., Jodeh, S., Hanbali, G., Safi, Z., Berisha, A., Xhaxhiu, K., et al. (2022). Eco-Friendly synthesis and characterization of double-crossed link 3D graphene oxide functionalized with chitosan for adsorption of sulfamethazine from aqueous solution: experimental and DFT calculations. *Front. Environ. Sci.* 10, 977. doi:10.3389/fenvs.2022.930693

Hanelt, S., Orts-Gil, G., Friedrich, J. F., and Meyer-Plath, A. (2011). Differentiation and quantification of surface acidities on MWCNTs by indirect potentiometric titration. *Carbon* 49, 2978–2988. doi:10.1016/j.carbon.2011.03.016

Hiew, B. Y. Z., Lee, L. Y., Lai, K. C., Gan, S., Thangalazhy-Gopakumar, S., Pan, G.-T., et al. (2019). Adsorptive decontamination of diclofenac by three-dimensional graphene-based adsorbent: response surface methodology, adsorption equilibrium, kinetic and thermodynamic studies. *Environ. Res.* 168, 241–253. doi:10.1016/j.envres.2018.09.030

Hiew, B. Y. Z., Tee, W. T., Loh, N. Y. L., Lai, K. C., Hanson, S., Gan, S., et al. (2022). Synthesis of a highly recoverable 3D MnO2/rGO hybrid aerogel for efficient adsorptive separation of pharmaceutical residue. *J. Environ. Sci.* 118, 194–203. doi:10.1016/j.jes.2021.12.036

Hohenberg, P., and Kohn, W. (1964). Inhomogeneous electron gas. *Phys. Rev.* 136, B864–B871. doi:10.1103/physrev.136.b864

Huang, P., Jia, H., Wang, T., Xu, Y., Zhang, L., Wei, X., et al. (2021). Effects of modification degrees on the colloidal stability of amphiphilic janus graphene oxide in aqueous solution with and without electrolytes. *Langmuir* 37, 10061–10070. doi:10.1021/acs.langmuir.1c01283

Jauris, I., Matos, C. F., Zarbin, A. J. G., Umpierres, C. S., Saucier, C., Lima, E. C., et al. (2017). Adsorption of anti-inflammatory nimesulide by graphene materials: a combined theoretical and experimental study. *Phys. Chem. Chem. Phys.* 19, 22099–22110. doi:10.1039/c7cp04272h

Jung, H., Cho, K. M., Kim, K. H., Yoo, H.-W., Al-Saggaf, A., Gereige, I., et al. (2018). Highly efficient and stable CO2 reduction photocatalyst with a hierarchical structure of mesoporous TiO2 on 3D graphene with few-layered MoS2. *ACS Sustain. Chem. Eng.* 6, 5718–5724. doi:10.1021/acssuschemeng.8b00002

Kohn, W., and Sham, L. J. (1965). Self-consistent equations including exchange and correlation effects. *Phys. Rev.* 140, A1133–A1138. doi:10.1103/physrev.140.a1133

Kristensen, D. M., Hass, U., Lesné, L., Lottrup, G., Jacobsen, P. R., Desdoits-Lethimonier, C., et al. (2011). Intrauterine exposure to mild analgesics is a risk factor for development of male reproductive disorders in human and rat. *Hum. Reprod.* 26, 235–244. doi:10.1093/humrep/deq323

Kristensen, D. M., Lesné, L., Le Fol, V., Desdoits-Lethimonier, C., Dejucq-Rainsford, N., Leffers, H., et al. (2012). Paracetamol (acetaminophen), aspirin (acetylsalicylic acid) and indomethacin are anti-androgenic in the rat foetal testis. *Int. J. Androl.* 35, 377–384. doi:10.1111/j.1365-2605.2012.01282.x

Kristensen, D. M., Mazaud-Guittot, S., Gaudriault, P., Lesné, L., Serrano, T., Main, K. M., et al. (2016). Analgesic use—prevalence, biomonitoring and endocrine and reproductive effects. *Nat. Rev. Endocrinol.* 12, 381–393. doi:10.1038/nrendo.2016.55

Leão, M. B., Rosa, P. C., Dalla Corte, C. L., and Matos, C. F. (2022). Eco-friendly, non-toxic and super adsorbent hydrogels based on graphene. *Mater. Chem. Phys.* 288, 126408. doi:10.1016/j.matchemphys.2022.126408

Leão, M. B., Vendrame, L., Fagan, S. B., Zanella, I., Jauris, I. M., Bordin, J. R., et al. (2023). Combining multi-scale simulations and experiments to unveil the adsorption of methylene blue in graphene tridimensional-based materials. *Mol. Syst. Des. Eng.* 8, 666–680. doi:10.1039/d2me00268j

Lima, É. C., Adebayo, M. A., and Machado, F. M. (2015). "Kinetic and equilibrium models of adsorption," in *Carbon nanomaterials as adsorbents for environmental and biological applications* (Berlin, Germany: Springer), 33–69.

Lin, Y., Tian, Y., Sun, H., and Hagio, T. (2021). Progress in modifications of 3D graphene-based adsorbents for environmental applications. *Chemosphere* 270, 129420. doi:10.1016/j.chemosphere.2020.129420

Liu, H., and Qiu, H. (2020). Recent advances of 3D graphene-based adsorbents for sample preparation of water pollutants: a review. *Chem. Eng. J.* 393, 124691. doi:10.1016/j.cej.2020.124691

Liu, X., Ma, R., Wang, X., Ma, Y., Yang, Y., Zhuang, L., et al. (2019). Graphene oxide-based materials for efficient removal of heavy metal ions from aqueous solution: a review. *Environ. Pollut.* 252, 62–73. doi:10.1016/j.envpol.2019.05.050

Lorphensri, O., Intravijit, J., Sabatini, D. A., Kibbey, T. C., Osathaphan, K., and Saiwan, C. (2006). Sorption of acetaminophen, 17α-ethynyl estradiol, nalidixic acid, and norfloxacin to silica, alumina, and a hydrophobic medium. *Water Res.* 40, 1481–1491. doi:10.1016/j.watres.2006.02.003

Lu, Y., Li, Y., Gao, Y., Ai, B., Gao, W., and Peng, G. (2020). Facile preparation of 3D GO with caffeic acid for efficient adsorption of norfloxacin and ketoprofen. *Water Sci. Technol.* 81, 1461–1470. doi:10.2166/wst.2020.193

Moussavi, G., Hossaini, Z., and Pourakbar, M. (2016). High-rate adsorption of acetaminophen from the contaminated water onto double-oxidized graphene oxide. *Chem. Eng. J.* 287, 665–673. doi:10.1016/j.cej.2015.11.025

Paredes-Laverde, M., Salamanca, M., Silva-Agredo, J., Manrique-Losada, L., and Torres-Palma, R. A. (2019). Selective removal of acetaminophen in urine with activated carbons from rice (Oryza sativa) and coffee (Coffea arabica) husk: effect of activating agent, activation temperature and analysis of physical-chemical interactions. *J. Environ. Chem. Eng.* 7, 103318. doi:10.1016/j.jece.2019.103318

Sankey, O. F., and Niklewski, D. J. (1989). *Ab initio* multicenter tight-binding model for molecular-dynamics simulations and other applications in covalent systems. *Phys. Rev. B* 40, 3979–3995. doi:10.1103/physrevb.40.3979

Shan, D., Deng, S., Li, J., Wang, H., He, C., Cagnetta, G., et al. (2017). Preparation of porous graphene oxide by chemically intercalating a rigid molecule for enhanced removal of typical pharmaceuticals. *Carbon* 119, 101–109. doi:10.1016/j.carbon.2017.04.021

Soler, J. M., Artacho, E., Gale, J. D., García, A., Junquera, J., Ordejón, P., et al. (2002). The SIESTA method for *ab initio* order-N materials simulation. *J. Phys. Condens. Matter* 14, 2745–2779. doi:10.1088/0953-8984/14/11/302

Soltani, R., Marjani, A., and Shirazian, S. (2019). Facile one-pot synthesis of thiol-functionalized mesoporous silica submicrospheres for Tl (I) adsorption: isotherm, kinetic and thermodynamic studies. *J. Hazard. Mater.* 371, 146–155. doi:10.1016/j.jhazmat.2019.02.076

Song, C., Guo, B.-B., Sun, X.-F., Wang, S.-G., and Li, Y.-T. (2019). Enrichment and degradation of tetracycline using three-dimensional graphene/MnO2 composites. *Chem. Eng. J.* 358, 1139–1146. doi:10.1016/j.cej.2018.10.119

Sun, H., Lin, Y., Takeshi, H., Wang, X., Wu, D., and Tian, Y. (2021). Synthesis of 3D graphene-based materials and their applications for removing dyes and heavy metals. *Environ. Sci. Pollut. Res.* 28, 52625–52650. doi:10.1007/s11356-021-15649-w

Thue, P. S., Sophia, A. C., Lima, E. C., Wamba, A. G., de Alencar, W. S., dos Reis, G. S., et al. (2018). Synthesis and characterization of a novel organic-inorganic hybrid clay adsorbent for the removal of acid red 1 and acid green 25 from aqueous solutions. *J. Clean. Prod.* 171, 30–44. doi:10.1016/j.jclepro.2017.09.278

Torabi Fard, N., Tadayon, F., Ahmad Panahi, H., and Moniri, E. (2022). Synthesize, characterization and application of a novel three-dimensional magnetic graphene oxide decorated with polyester dendrimers for detection of donepezil hydrochloride in pharmaceutical formulation and biological fluid. *Synth. Met.* 290, 117141. doi:10.1016/j.synthmet.2022.117141

Troullier, N., and Martins, J. L. (1991). Efficient pseudopotentials for plane-wave calculations. *Phys. Rev. B* 43, 1993–2006. doi:10.1103/physrevb.43.1993

Umbreen, N., Sohni, S., Ahmad, I., Khattak, N. U., and Gul, K. (2018). Self-assembled three-dimensional reduced graphene oxide-based hydrogel for highly efficient and facile removal of pharmaceutical compounds from aqueous solution. *J. colloid interface Sci.* 527, 356–367. doi:10.1016/j.jcis.2018.05.010

van den Driesche, S., Macdonald, J., Anderson, R. A., Johnston, Z. C., Chetty, T., Smith, L. B., et al. (2015). Prolonged exposure to acetaminophen reduces testosterone production by the human fetal testis in a xenograft model. *Sci. Transl. Med.* 7, 288ra80. doi:10.1126/scitranslmed.aaa4097

Vendrame, L. F., Zuchetto, T., Fagan, S. B., and Zanella, I. (2019). Nanofilter based on functionalized carbon nanostructures for the adsorption of pentachlorophenol molecules. *Comput. Theor. Chem.* 1165, 112561. doi:10.1016/j.comptc.2019.112561

Vijayaraghavan, K., Padmesh, T., Palanivelu, K., and Velan, M. (2006). Biosorption of nickel (II) ions onto Sargassum wightii: application of two-parameter and three-parameter isotherm models. *J. Hazard. Mater.* 133, 304–308. doi:10.1016/j.jhazmat.2005.10.016

Villaescusa, I., Fiol, N., Poch, J., Bianchi, A., and Bazzicalupi, C. (2011). Mechanism of paracetamol removal by vegetable wastes: the contribution of π–π interactions, hydrogen bonding and hydrophobic effect. *Desalination* 270, 135–142. doi:10.1016/j.desal.2010.11.037

Wang, J., Duan, X., Dong, Q., Meng, F., Tan, X., Liu, S., et al. (2019). Facile synthesis of N-doped 3D graphene aerogel and its excellent performance in catalytic degradation of antibiotic contaminants in water. *Carbon* 144, 781–790. doi:10.1016/j.carbon.2019.01.003

Wang, J.-b., Ren, Z., Hou, Y., Yan, X.-l., Liu, P.-z., Zhang, H., et al. (2020). A review of graphene synthesis at low temperatures by CVD methods. *New Carbon Mater.* 35, 193–208. doi:10.1016/s1872-5805(20)60484-x

Wong, L. Y., Lau, S. Y., Pan, S., and Lam, M. K. (2022). 3D graphene-based adsorbents: synthesis, proportional analysis and potential applications in oil elimination. *Chemosphere* 287, 132129. doi:10.1016/j.chemosphere.2021.132129

Wong, S., Lim, Y., Ngadi, N., Mat, R., Hassan, O., Inuwa, I. M., et al. (2018). Removal of acetaminophen by activated carbon synthesized from spent tea leaves: equilibrium, kinetics and thermodynamics studies. *Powder Technol.* 338, 878–886. doi:10.1016/j.powtec.2018.07.075

Yang, Y., Liu, Y., Fang, X., Miao, W., Chen, X., Sun, J., et al. (2020). Heterogeneous Electro-Fenton catalysis with HKUST-1-derived Cu@ C decorated in 3D graphene network. *Chemosphere* 243, 125423. doi:10.1016/j.chemosphere.2019.125423

Yanyan, L., Kurniawan, T. A., Albadarin, A. B., and Walker, G. (2018). Enhanced removal of acetaminophen from synthetic wastewater using multi-walled carbon nanotubes (MWCNTs) chemically modified with NaOH, HNO3/H2SO4, ozone, and/or chitosan. *J. Mol. Liq.* 251, 369–377. doi:10.1016/j.molliq.2017.12.051

Yousefi, N., Lu, X., Elimelech, M., and Tufenkji, N. (2019). Environmental performance of graphene-based 3D macrostructures. *Nat. Nanotechnol.* 14, 107–119. doi:10.1038/s41565-018-0325-6

Yu, Z., Wei, L., Lu, L., Shen, Y., Zhang, Y., Wang, J., et al. (2022). Structural manipulation of 3D graphene-based macrostructures for water purification. *Gels* 8, 622. doi:10.3390/gels8100622